Advanced Fiber Materials (2022) 4:1595–1608
https://doi.org/10.1007/s42765-022-00192-1

RESEARCH ARTICLE

Waste Textile Reutilization Via a Scalable Dyeing Technology: A Strategy to Enhance Dyestuffs Degradation Efficiency

Heng Zhai[1] · Zekun Liu[1] · Lulu Xu[1] · Ting Liu[1] · Yangyang Fan[1] · Lu Jin[1] · Ruihan Dong[1] · Yangpeiqi Yi[1] · Yi Li[1]

Received: 27 March 2022 / Accepted: 1 August 2022 / Published online: 7 September 2022

Abstract

The rapid expansion of the fast fashion industry brings about environmental concerns such as dyestuffs-related water pollutions and waste textiles. Conventional wastewater-disposal strategies emphasize the optimization of photocatalytic activity to improve pollutant degradation efficiency, while the absorptivity, recyclability and sustainability of photocatalysts are always ignored. The overproduced textiles are still in urgent of being recycled and reutilized in eco-friendly approaches. In this work, a scalable dyeing technology is employed to achieve green and sustainable reutilization of waste textiles. The functionalized TiO_2/reduced graphene oxide wool fabrics show excellent sustainability, remarkable adsorbing capacity and enhanced photocatalytic performance. By taking advantage of these properties, we develop an integrated strategy of night-time adsorption and day-time photodegradation which could significantly optimize the dyestuffs degradation efficiency. The concept of waste textiles reutilization and wastewater treatment in this work provides practical potential for efficient and sustainable environmental remediation.

Keywords Waste textile reutilization · Wastewater treatment · Adsorption · Photocatalysis

Introduction

Nowadays, water pollution has been paid much attention due to the crisis of water resources. The textile industry is estimated to be responsible for approximately 20% of global clean water pollution arising from dyeing and finishing production [1]. Especially the rapid development of fast fashion market, which leads to increasing overproduction and overconsumption of textiles, accelerating the water contamination by organic dyestuffs [2]. To address the water pollution concerns, the conversion of solar energy to degrade pollutants in water has been considered as one of the most efficient and effective solutions. Photocatalysts such as TiO_2 nanoparticles are widely employed due to their high catalytic stability, cost-effective property and moderate demands for the ambient condition [3–5]. However, the fast recombination rate of photogenerated electron–hole (e^-/h^+) pairs and weak adsorbing affinity of nanoparticles toward target contaminants restrict the photocatalytic performance of TiO_2, and affect the overall degradation efficiency [6, 7]. Moreover, the particle-based TiO_2 photocatalysts tend to sink down into the water, which reduces their recyclability and sustainability in practical applications.

Recent studies put more emphasis on optimizing the pollutant degradation efficiency of TiO_2 by improving its photocatalytic performance. This was achieved through various doping materials, including metallic doping, non-metallic doping and noble-metal loading [8, 9]. Among these doping materials, carbonaceous materials such as carbon nanotube and graphene are more favorable owing to their superior properties in transporting electrons, good optical transmittance, large specific surface and strong adsorption capacity [10–13]. The integration of graphene and TiO_2 improves the photocatalytic performance of TiO_2 by increasing utilization rates of solar energy and prolonging lifetime of electron–hole pairs [14, 15]. However, the photocatalysts would no longer photodegrade contaminations without the participation of illuminations, such as on heavy cloudy days or even at night. Enhancing the adsorbing affinity of photocatalysts towards pollutants and taking full advantage of night-time adsorption as alternative ways to accelerate pollutant degradation are always ignored. It is highly desirable to fabricate recyclable and sustainable photocatalysts with

✉ Yi Li
henry.yili@manchester.ac.uk

[1] Department of Materials, University of Manchester, Oxford Road, Manchester M13 9PL, UK

massive absorption towards pollutants at night and enhanced photocatalytic performance to optimize the overall degradation efficiency.

On the other hand, the fast fashion industry generates approximately 92 million tons of textile wastes annually around the world, most of which end up in landfills or incinerations [16]. Even though reuse and recycle of waste textiles as environmentally-friendly solutions have been put forward, there are only a small amount of intact textiles that can be reused in the conventional ways through donating, swapping and reselling [17]. For those obsolescent garments which are not suitable to wear, their fabrics and fibres can be separated and recycled into new products by chemical dissolution and remanufacture [18, 19]. The challenges in the separations of blending fibres such as cotton/polymer and wool/polymers and potential secondary pollution in chemical dissolution of synthetic fibres hinder the effective and sustainable recycles of waste garments. To date, it still leaves a vacancy to reutilize waste textiles in a green manner.

Herein, we propose a scalable dyeing technology to synchronously realize the sustainable reutilization of waste textiles and efficient degradation of dyestuffs in wastewater. The TiO_2/reduced graphene oxide (rGO) functionalized fabrics originated from waste wool fabrics exhibit the splendid adsorbing ability and enhanced photocatalytic performance, with a maximum adsorbing capacity of 427.35 mg/g to methylene blue (MB) analyzed by Langmuir adsorption isotherms, and complete photodegradation of MB (100 mL, 10 mg/L) within 60 min under 150 W Xenon lamp. Notably, by integrating night-time absorption prior to photodegradation, the overall photodegradation could be shortened to 30 min. The strong bonding between TiO_2/rGO composites and fabric substrates ensures the functionalized fabrics can stably and sustainably photodegrade dyestuffs in aqueous solution.

Experimental Section

Preparation of GO Dispersion and TiO_2/GO Composite Dispersion

Graphene oxide dispersion was prepared from expandable graphite flakes by a modified Hummers method which has been introduced in my previous work [20, 21]. 0.5 g expandable graphite was heated at 750 W in the microwave oven for 30 s to form expanded graphite. Then expanded graphite, H_2SO_4 (100 mL, 98 wt%) and $KMnO_4$ (5 g) were mixed and stirred for 24 h. The mixture was slowly diluted with 100 mL deionized water in an ice bath and followed by H_2O_2 (10 mL 35 wt%). HCl (100 mL 10 wt%) was then added to the mixture. Finally, graphene oxide was obtained after being centrifuged. The TiO_2 nanoparticles were purchased from Sigma-Aldrich. 1000 mg TiO_2 nanoparticles were dispersed in 50 mL deionized water to obtain 20 mg/mL TiO_2 dispersion. Different mass of dry GO (52.63 mg, 111 mg, 176 mg and 250 mg) was added to TiO_2 dispersion to form 4 groups of TiO_2/GO dispersion (TiO_2/5%GO, TiO_2/10% GO, TiO_2/15%GO and TiO_2/20%GO). The TiO_2/GO dispersions were then well dispersed by ultrasonication at 50 ℃ for 4 h.

Pad Dyeing of Wool Fabric

Before the pad-dying process, the pristine wool fabric substrate was pre-washed in deionized water and dried in the oven. The TiO_2/GO composite dispersion was transferred into the bath of the pad-dyeing machine. Each pristine wool fabric was padded 3 cycles in the machine and dried in the oven at 60 ℃ after each cycle. To ensure the GO/TiO_2 composites were firmly and stably coated on the fabric surface, the coated wool fabrics were immersed in the L-ascorbic acid (L-AA) solvent in a water bath at 80 ℃ for 24 h. The L-AA acid treatment induced the reduction of the graphene oxide on the surface. Finally, the functionalized fabrics were achieved.

Dark Adsorption Test

Dark adsorption experiment was carried out in a dark environment and at room temperature (20 °C) by immersing TiO_2/rGO coated wool fabrics into 100 mL MB solutions with different concentrations ranging from 5 to 20 mg/L. The adsorption equilibrium was reached when the concentration of MB solutions kept stable. The adsorption capacity was calculated using the following equation:

$$q_e = \left(\frac{C_0 - C_e}{m}\right) \times V \quad (1)$$

where C_0 and C_e represent the initial and equilibrium concentrations of MB (mg/L) respectively, m stands for the mass of TiO_2/rGO composites (g) and V is the volume of the solution (L).

Photocatalytic Degradation Measurements

All the photocatalytic experiments were carried out under a 150 W Xenon lamp (PLS-SXE300, Beijing Perfect light Co., Ltd). TiO_2/rGO functionalized fabrics were immersed in 100 mL MB solution with an initial concentration of 10 mg/L. The irradiation was given out immediately once photocatalysts were settled down to avoid any dark adsorptions. The vertical distance between the solution plane level and lamp was fixed at 10 cm (Fig. S5). For comparison, photocatalytic degradation of MB in the presence of pure TiO_2 coated wool fabrics was also studied under the same

conditions. The concentration of MB was recorded at the same interval time and analyzed using M550 UV/Visible Spectrophotometer. The degradation rates were calculated by the equation below:

$$\eta(\%) = 1 - \left(\frac{A}{A_0}\right) \times 100\% \quad (2)$$

where A_0 and A are the initial and remaining concentration of MB.

Characterization of the TiO_2/rGO Coated Wool Fabric

The surface morphology and crystal structure were characterized by Zeiss Ultra 55 Scanning Electron Microscope (SEM) and FEI Tecnai T20 Transmission Electron Microscope (TEM). The elemental analysis and mapping of TiO_2/rGO Coated fabric were analyzed from an energy-dispersive X-ray spectrometer (EDX) by FEI Quanta 250. The Raman spectra of the TiO_2/GO and TiO_2/rGO coated fabrics were carried out using a Horiba Raman spectrometer with a 633 nm excitation wavelength. The X-ray diffraction (XRD) patterns were recorded on an XRD5 spectrometer (Type PANaytical X'Pert Pro) at operating voltage of 40 kV and current at 40 mA using Cu Kα irradiation. The Fourier transform infrared (FTIR) spectra were recorded by Bruker Hyperion 3000 IR Microscope. X-ray photoelectron spectroscopy (XPS) was measured by ESCALAB 250 Xi. Photoluminescence (PL) emission spectra were obtained from LabRam HR Evolution with a 325 nm edge filter.

Results and Discussion

Preparation of Functionalized Fabrics

Figure 1 shows the basic concept that waste textiles are reutilized in wastewater treatment. The fast fashion industries take responsibility for the large amounts of waste textiles and dyestuffs-related wastewater. Herein, these overproduced textiles could be transferred into TiO_2/rGO functionalized fabrics with abundant adsorption and enhanced photocatalytic property through pad dyeing technology. The dyestuff molecules in textile wastewater are massively absorbed on the surface of functionalized fabrics and photodegraded in a green approach.

The reutilization of waste fabrics is illustrated in Fig. 2a, which exhibits the fabrication of TiO_2/rGO functionalized fabrics from pieces of wool fabrics by pad dyeing technology. The graphene oxide (GO) was synthesized from expandable graphite according to our previous papers [22, 23]. We introduce the pad dyeing approach, which provides considerable force from two spinning compression rollers, to assist the TiO_2/rGO nanoparticles firmly and stably coated

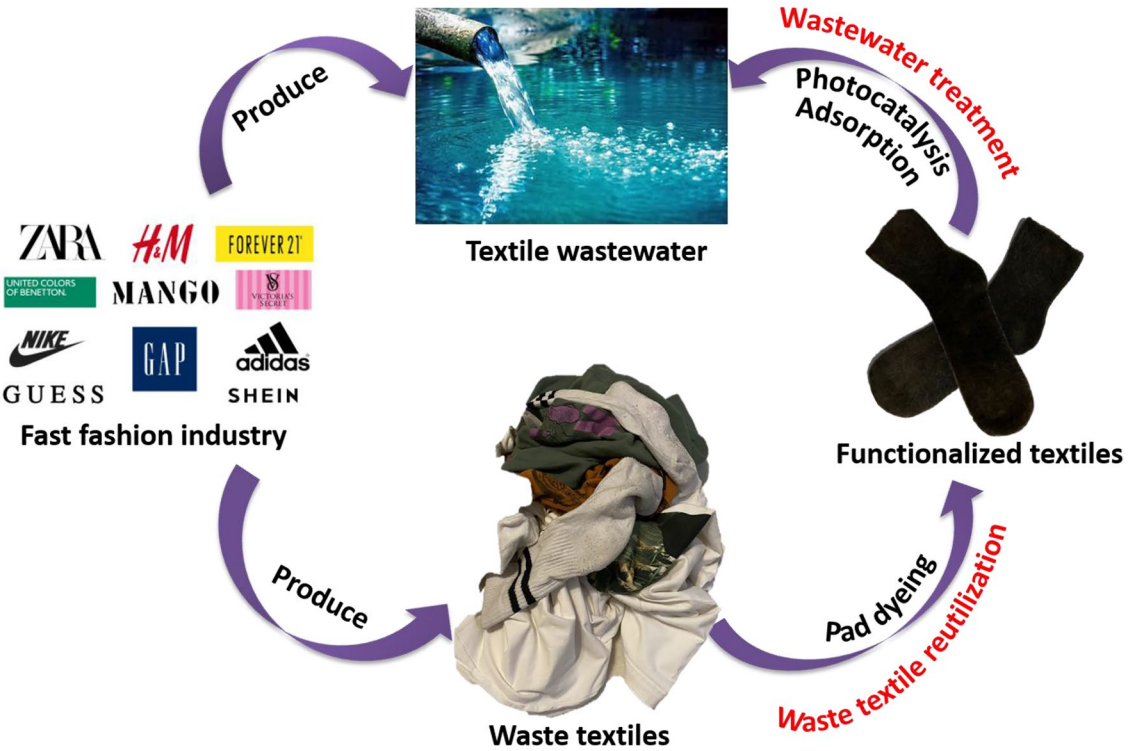

Fig. 1 Concept of waste textiles reutilization and wastewater treatment

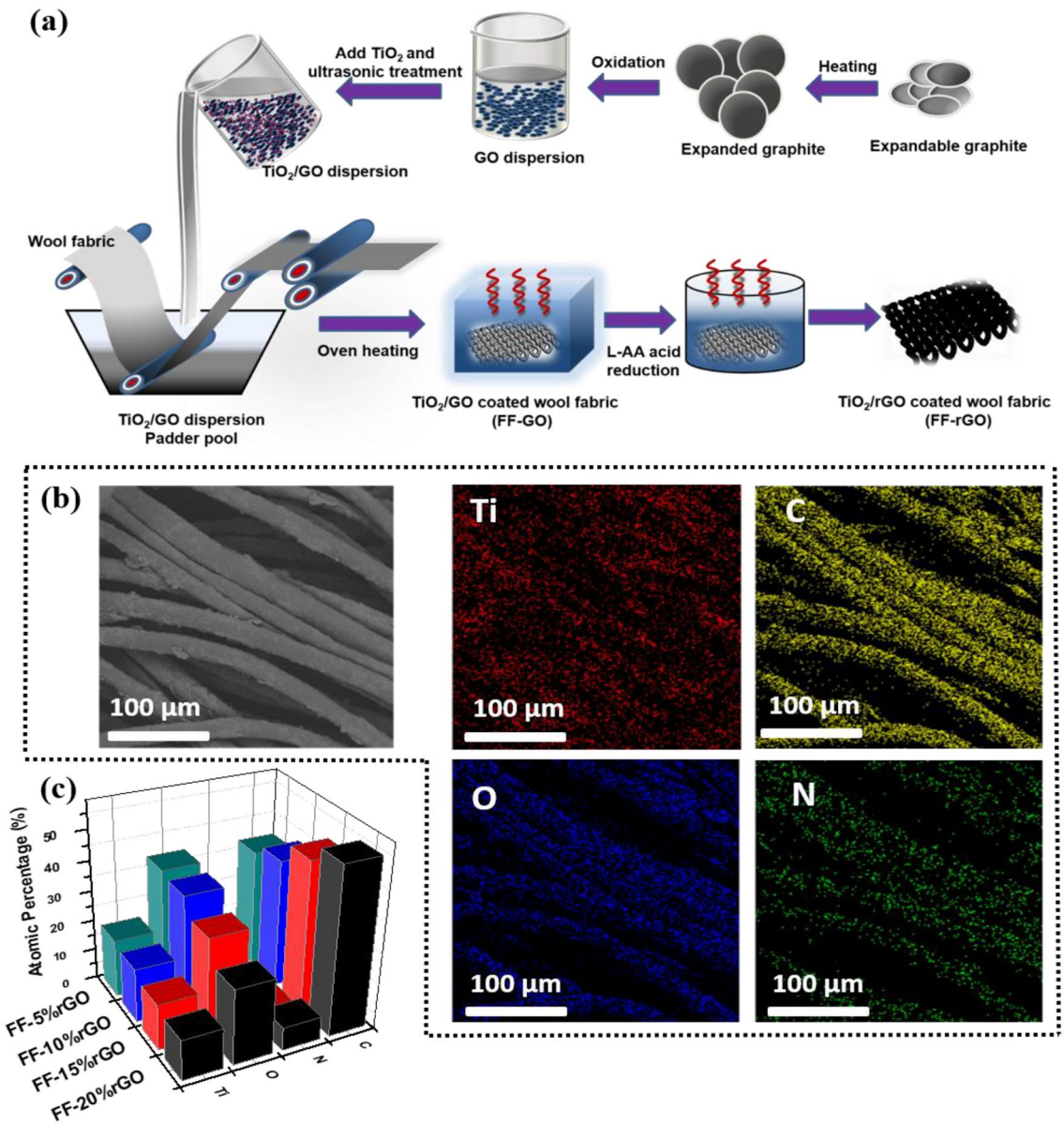

Fig. 2 **a** Schematic illustration of the fabrication of FF-rGO. **b** EDX mapping images of FF-20%rGO. **c** The surface elements in various FF-rGO

on the surface of fabrics. Finally, the functionalized fabrics coated by TiO_2/5%rGO, TiO_2/10%rGO, TiO_2/15%rGO, TiO_2/20%rGO and pure TiO_2 nanoparticles were achieved. They are defined as FF-5%rGO, FF-10%rGO, FF-15%rGO, FF-20%rGO and FF-TiO_2, respectively. The fabrications of GO and TiO_2/rGO functionalized fabric (FF-rGO) are explained in the experimental section. The images of pristine wool fabrics after pad dyeing and L-AA reduction are shown in Fig. S1. The tensile stress of FF-rGO has increased compared with pristine wool fabrics, which can be attributed to the binding forces between rGO sheets on the fabric surface (Fig. S2). The element distributions of Ti, C, N and O in FF-rGO were captured by EDX mapping (Fig. 2b and Fig. S3), where the elements are evenly distributed. The atom percentage of Ti decreases from 19.02 to 13.16% and O decreases from 38.95 to 24.59%, indicating more TiO_2 nanoparticles in FF-5%rGO than those in FF-20%rGO (Fig. 2c). Such results demonstrate the actual contents of TiO_2/rGO composite on the fabric surface were in excellent accordance with experimental expectation.

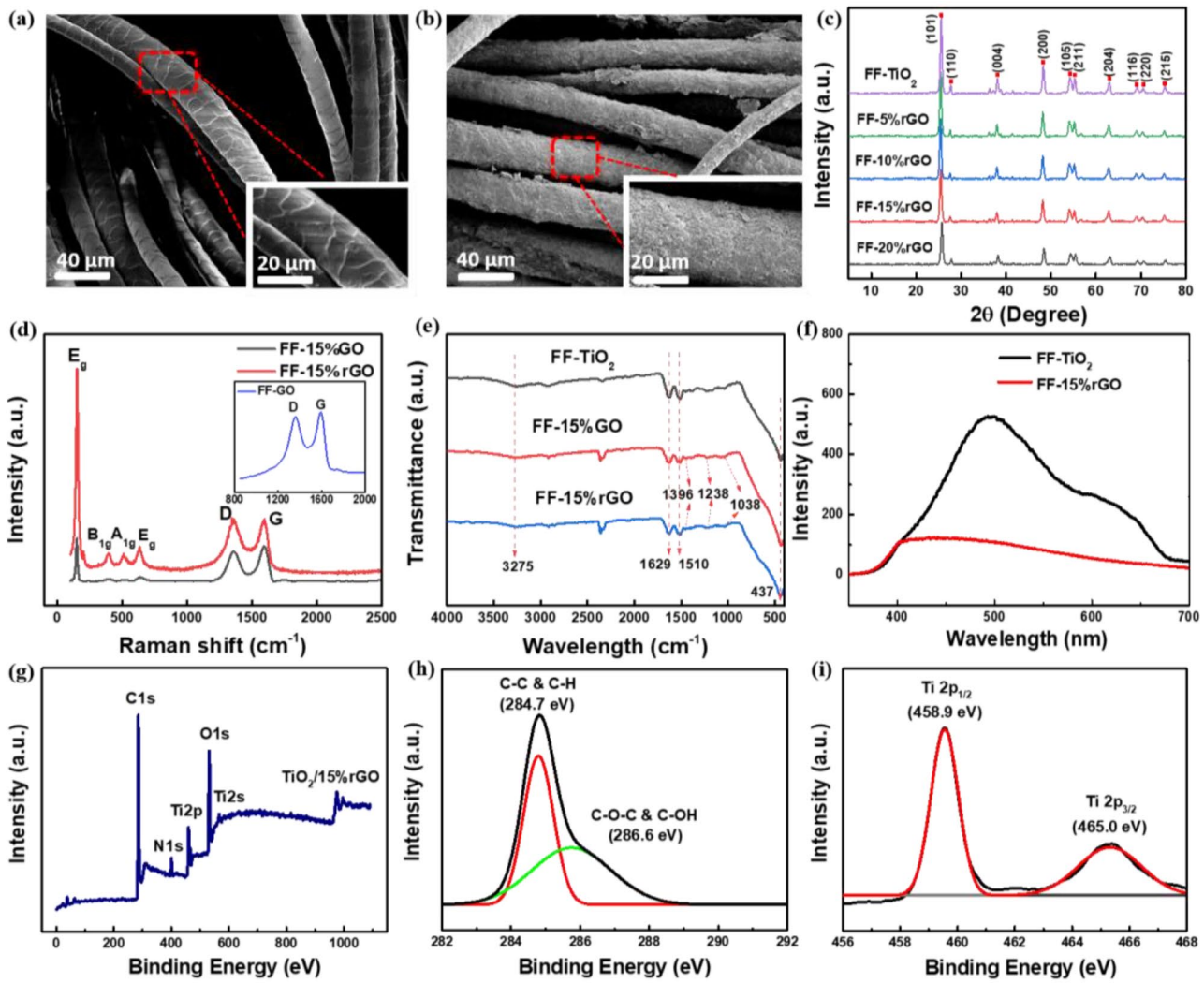

Fig. 3 Characterizations of FF-rGO. **a** SEM image of pristine wool fibres. **b** SEM image of FF-15%rGO. **c** XRD patterns of FF-rGO. **d** Raman spectra of FF-GO, FF-15%GO and FF-15%rGO. **e** FTIR spectra of FF-TiO_2, FF-15%GO and FF-15%rGO. **f** PL spectra of FF-TiO_2 and FF-15%rGO. **g** XPS spectra of FF-15%rGO. **h** Peak deconvolution of C (1s). **i** Peak deconvolution of Ti (2p)

Characterizations

Before pad dyeing, pristine wool fibre shows obvious overlapping scale structure (Fig. 3a). After dyeing and reduction of GO, it can be apparently observed that TiO_2/15% rGO particles have been homogenously and densely coated on the wool fibre surface (Fig. 3b). The high-magnification SEM image reveals TiO_2 nanoparticles are wrapped by rGO sheets on the fibre surface. TEM image in Fig. S4a confirms the coexistence of TiO_2 and rGO, with TiO_2 wrapped by transparent, layered rGO sheets. High-resolution TEM image further indicates the diameter of TiO_2 nanoparticles is around 50 nm which belongs to anatase TiO_2 (Fig. S4b) [24]. The diffraction peaks in the XRD patterns in Fig. 3c can be marked as (101), (004), (200), (105), (211), (204), (215) crystal planes of TiO_2 (JCPDS NO. 21-1272), which are corresponding to anatase phase [25]. The crystallite size was calculated by the Scherrer equation (result listed in Table S1). According to the analysis, the intensity of diffraction peaks decreases when incorporating rGO into TiO_2, indicating the formation of finer crystallite size. The finest grain size of TiO_2 is 15.84 nm from FF-15%rGO, which suggests that 15% rGO is more favorable to modify TiO_2 with finer crystallite size.

Figure 3d exhibits the Raman spectra of FF-GO, FF-15%GO and FF-15%rGO. The peaks at 156 (E_g), 399 (B_{1g}), 513 (A_{1g}) and 639 (E_g) cm^{-1} are ascribed to the anatase phase of TiO_2. The D band (peak at 1350 cm^{-1}) corresponds to the defects and disordered carbons while the G band (peak at 1595 cm^{-1}) contributes to ordered sp^2-bonded carbon [26]. The intensity ratio of the D and G band, recorded as I_D/I_G, was employed to measure the disorder and defects,

which is the main characteristic to influence electrical conductivity [27]. The I_D/I_G values of FF-GO, FF-15%GO and FF-15%rGO were calculated into 0.932, 0.948 and 1.017, respectively. Such results indicate the GO on the fabric surface has been slightly reduced by the incorporation of TiO_2 nanoparticles, while largely reduced into rGO when the chemical reduction method was applied. The electrical conductivity of rGO increased throughout the reduction, which would facilitate electron transferring from TiO_2 to rGO and hinder the recombination of electron–hole pairs.

By analyzing the FTIR spectra of FF- TiO_2, FF-15%GO and FF-15% rGO, we observed peaks around 3300 cm^{-1} which are corresponding to O–H stretching vibration of hydroxyl groups in all functionalized fabrics (Fig. 3e). The hydroxyl groups are beneficial to accept photo-induced holes and convert into ·OH radicals which significantly contributes to photocatalytic enhancement [28]. The presence of a peak at 1629 cm^{-1} is assigned to skeletal C=C vibration in rGO, which is corresponded to sp^2 character. Similar characters were observed for bands at 1238 and 1038 cm^{-1}, which are attributed to C–OH stretching vibration and C–O stretching vibration in the epoxy group, respectively [29]. The peaks at 1396 and 400–700 cm^{-1} suggest the presence of Ti–O–C and Ti–O–Ti respectively, indicating the formation of chemical interactions between functional groups in rGO and surface hydroxyl groups of TiO_2 nanoparticles [30].

Photoluminescence (PL) Spectra is widely employed to investigate the behaviors of photoinduced e^-/h^+ pairs, including trapping, immigration and transfer of charge carries [31]. PL phenomenon occurs due to the emitted photons, which is from the exceeded energy when the recombination of charge carrier takes place under irradiation. The weakened PL signal observed in FF-15%rGO in Fig. 3f indicates that photoelectrons were either trapped by defect sites (e.g., oxygen vacancies) or immigrating from TiO_2 surface to rGO sheets prior to their recombination with holes [32]. Under both circumstances, the recombination behavior of photoinduced e^-/h^+ pairs will be effectively blocked and the lifetime of charge carries will be promoted, accounting for enhanced photocatalytic activity in FF-15%rGO.

We further investigated the chemical nature of modified wool fabrics through XPS, which confirms the existence of C, N, O and Ti compositions in FF-15%rGO (Fig. 3g). The high resolution of C 1s XPS spectra (Fig. 3h) suggests the existence of C–C bond (284.7 eV) and C–O–C of the epoxy group (286.6 eV). The absence of C=O (carboxyl group) indicates GO in the composite has been reduced, which is in accordance with Raman results. The peaks located at 458.9 and 465.0 eV are related to Ti $2p_{1/2}$ and Ti $2p_{3/2}$ spin-orbital splitting photoelectrons from C–Ti bond (Fig. 3i), suggesting the chemical bond between TiO_2 and rGO has been well formed [33].

Absorbing Capacity of FF-rGO

The dark adsorption test was employed to measure the absorbing capability of FF-rGO without irradiations. The adsorption of pollutants such as MB is mostly based on physical interactions as shown in the theoretical schematic illustration (Fig. 4a). Electrostatic interaction as well as π-π stacking between MB molecular and functional groups in rGO play important roles in the generation of adsorbing behavior [34]. The adsorption isotherm of various FF-rGO was studied to quantitatively investigate the amount of MB molecular left in solution when the adsorption process reaches equilibrium. MB molecules are more favorably absorbed by the FF-rGO instead of FF-TiO_2 as shown in Fig. 4b. Especially for FF-15%rGO, whose equilibrating adsorbing capacity reaches 145.68 mg/g ($R^2 = 0.99$) at an initial MB concentration of 20 mg/L and is much larger than that of FF-TiO_2 (71.15 mg/g, $R^2 = 0.97$). The adsorbing ability increases with higher contents of rGO incorporated in FF-rGO from 5 to 15%. However, less MB molecule was absorbed even more rGO was incorporated (20%), which could be explained by the lower exposure of functional groups in FF-20%rGO caused by overlapping behavior of exceeded rGO sheets.

Several mathematical models have been implemented to describe the equilibrium of adsorption. The Langmuir model and Freundlich model are most frequently and widely spread among them. When applying the Langmuir model, there is a hypothesis that the uptake of dyes only occurs on a homogenous surface by monolayer adsorption [35]. The equation shows as:

$$\frac{C_e}{q_e} = \frac{C_e}{q_{max}} + \frac{1}{q_{max} K_L} \tag{3}$$

where q_{max} (mg/g) is the maximum adsorbing capacity corresponding to complete monolayer coverage, K_L (L/g) is a constant related to adsorption capacity and energy of adsorption. The results from Langmuir model in Fig. 4c show that the maximum adsorption for FF-15%rGO predicts to be 427.35 mg/g. The higher correction coefficients of R^2 ($R^2 = 0.957$) suggest the excellent fitting of experimental data by the Langmuir model, while FF-TiO_2 only obtains maximum adsorption with 80.76 mg/g ($R^2 = 0.978$). The dramatic improved maximum adsorbing capability indicates the great significance of 15%rGO incorporated in FF-rGO in adsorption enhancement of dyes, which is also confirmed by the comparative table of recent reports about adsorbing capacities of various adsorbents to MB (Table S2). While the Freundlich model assumes that the adsorption takes place on a heterogeneous surface [36]. The equation is represented by:

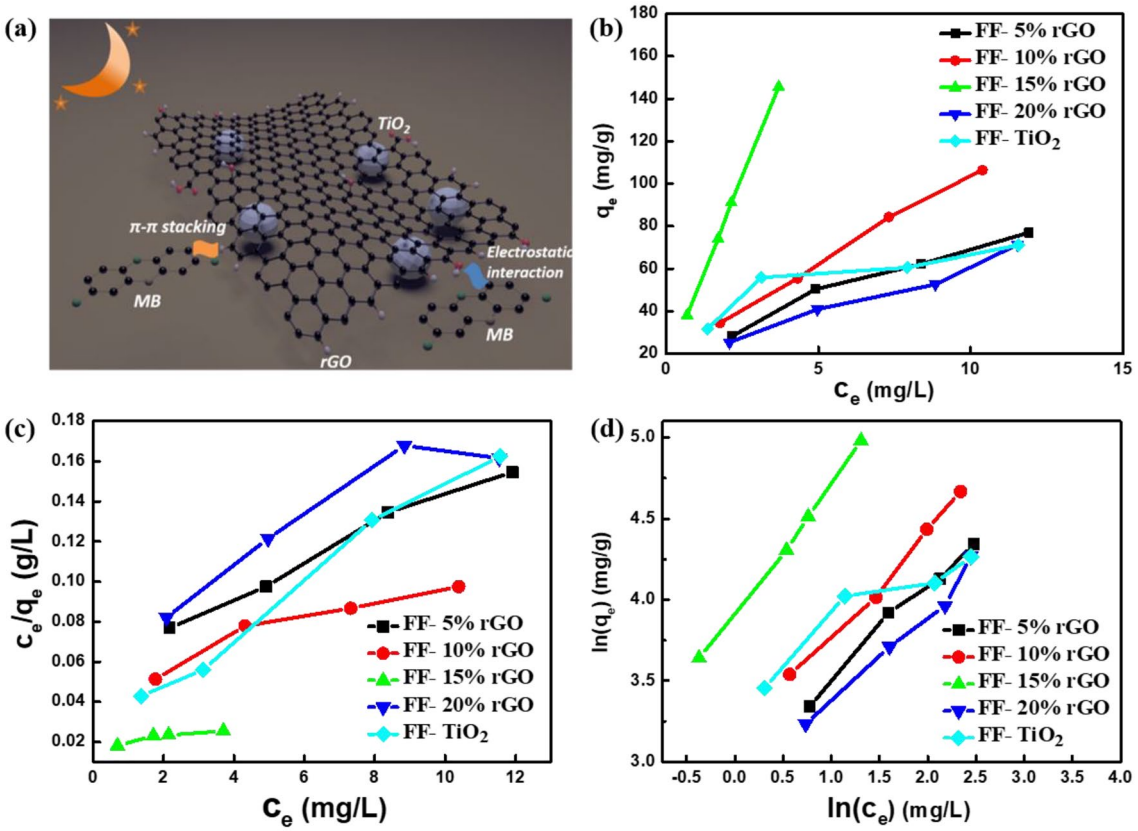

Fig. 4 **a** Schematic diagram of interactions between MB molecular and rGO sheets. **b** Adsorption isotherms of MB absorbed by FF-TiO_2 and FF-rGO under room temperature (20°C). **c** Adsorption isotherms of MB analyzed by Langmuir model. **d** Adsorption isotherms of MB analyzed by Freundlich model

$$Lnq_e = Lnk_f + \frac{1}{n}Lnc_e \quad (4)$$

where k_f (L/g) and n are the Freundlich constants, representing adsorption capacity and adsorption intensity respectively. The calculated values from the Freundlich model in Fig. 4d show an improved adsorption capacity of FF-15%rGO (k_f=1.37 L/g, R^2=0.998). The values of n are all between 1 and 10, indicating MB molecules are favorable adsorbed both on FF-TiO_2 and FF-rGO. The lower R^2 of FF-TiO_2 in the Freundlich model (R^2=0.811) than that in the Langmuir model (R^2=0.978) suggests the adsorption activity of FF-TiO_2 takes place most likely on a homogenous surface. On the contrary, FF-20%rGO exhibits totally opposite results with a lower R^2 (R^2=0.821) in the Langmuir model and higher R^2 (R^2=0.969) in the Freundlich model, as represented in Table S3. Such results suggest more rGO sheets were wrapped on the fabrics to form heterogeneous surfaces and these extra rGO sheets make negative effects to the adsorption of MB.

Enhanced Photocatalytic Performance of FF-rGO

The photocatalytic performance of FF-rGO was evaluated by degrading MB solution under a 150 W Xenon lamp as shown in Fig. S5. For comparison, FF-TiO_2 was evaluated under the same condition to discover the influences of rGO on the overall photocatalytic activity. The curves of MB degradation against time with different functionalized fabrics indicate the photocatalytic degradation performance has been improved when the fabrics were incorporated with rGO (Fig. 5a). More specifically, more than 80% of MB was removed after 30 min's photocatalysis and 95% of MB was removed after 60 min's photocatalysis in terms of FF-15%rGO, while these degradation rates decline to 50% for 30 min's photocatalysis and 80% for 60 min's photocatalysis in terms of FF-TiO_2, respectively. The photocatalytic efficiency has almost doubled due to the presence of rGO in TiO_2/15%rGO composite. Although when increasing rGO content to 20%, the photocatalytic efficiency of FF-20%rGO was slightly decreased compared with that of FF-15%rGO. This is mostly because the extra rGO sheets brought about blockage between the light and TiO_2 nanoparticles, resulting

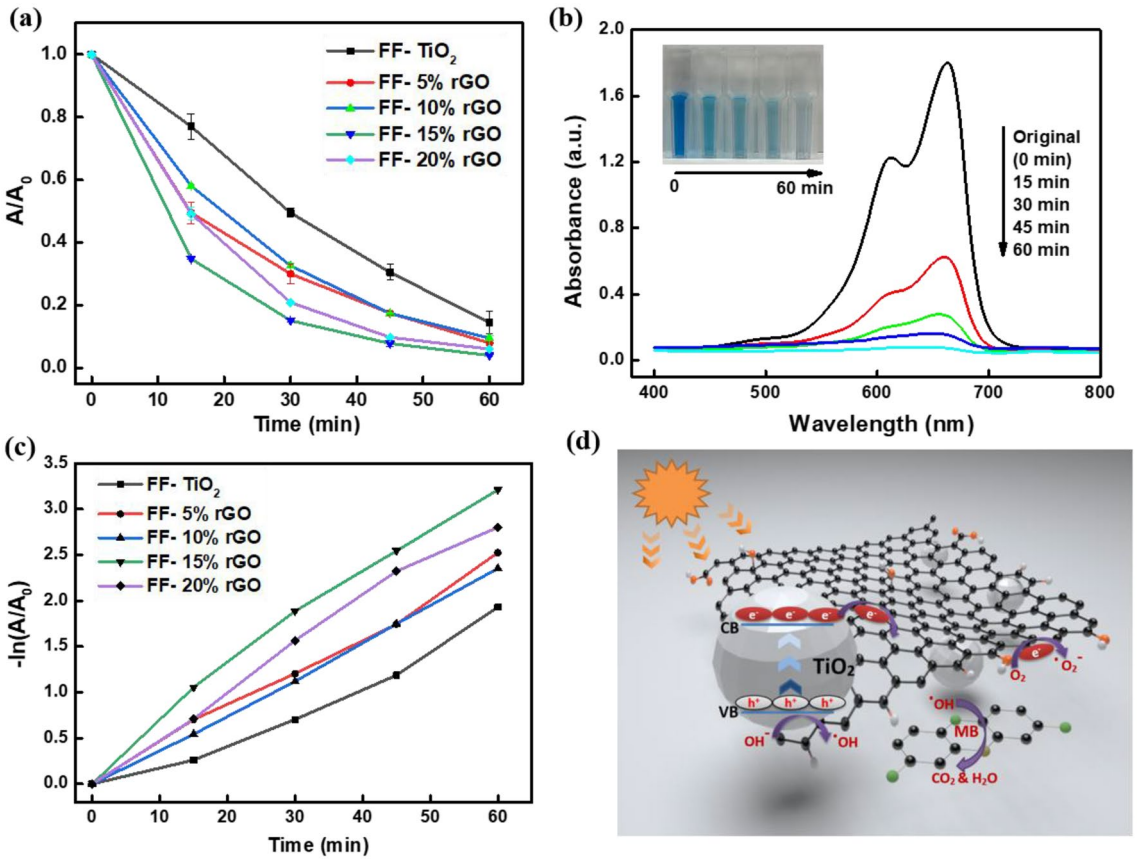

Fig. 5 **a** The photocatalytic degradation of MB over different functionalized fabrics. **b** The absorption spectra of MB photodegraded by FF-15%rGO. **c** Kinetic linear simulation curves for photodegradation of MB over different fabrics. **d** Schematic diagram showing electron transporting path during photodegradation of MB

in luminous energy loss in the transporting process. Figure 5b presents the UV–Vis adsorption spectra of MB aqueous during photodegradation for FF-15%rGO. The continuous decrease of the characteristic peak at 664 nm indicates the photodegradation was in progress. The sharp decrease of MB characteristic peak in the first 30 min suggests the degradation rate was fast at the beginning due to the abundant MB in the aqueous. The color of MB changed from blue to colorless demonstrates the chromophore of MB was removed and the benzene rings were cracked down during the photodegradation process (Fig. 5b) [37].

To have better understanding of photocatalytic efficiency regarding the above photocatalysis. The photocatalytic degradation kinetics was investigated by pseudo-first-order kinetics [38], represented as:

$$Ln\frac{A}{A_0} = kt \tag{5}$$

where k is the photocatalytic reaction apparent rate constant and t is the irradiation time. The slopes of curves in Fig. 5c were calculated as 0.0319 ($R^2 = 0.958$), 0.0406 ($R^2 = 0.992$), 0.0394 ($R^2 = 0.999$), 0.0528 ($R^2 = 0.985$) and 0.0481 ($R^2 = 0.990$) for FF-TiO_2, FF-5%rGO, FF-10%rGO, FF-15%rGO and FF-20%rGO, respectively. The k values of FF-rGO are much higher than that of FF-TiO_2, which further proves the introduction of rGO has significant effects on photocatalytic enhancement.

The improved photocatalysis was beneficial from the incorporation of rGO which extends the lifetimes of separated electron–hole pairs by providing alternative paths for electron transportation. During the photocatalysis, MB was mainly degraded by photoinduced holes (h^+_{VB}) and oxygen active species ($\cdot OH$ and $\cdot O_2^-$), which are derived from TiO_2 photocatalysts under irradiation [39]. The schematic mechanism of the photodegradation process of MB by FF-rGO is illustrated in Fig. 5d. Electrons (e^-) were firstly promoted from the valence band (VB) to the conduction band (CB) of TiO_2 under light irradiation, leaving holes (h^+_{VB}) with positive charges in the VB. The photoinduced electrons could immediately react with oxygen (O_2) to create superoxide radical ($\cdot O_2^-$), which is presented by:

$$TiO_2 + h\upsilon \rightarrow e^-_{CB} + h^+_{VB} \quad (6)$$

$$e^-_{CB} + O_2 \rightarrow \cdot O_2^- \quad (7)$$

Alternatively, by the presence of rGO sheets, electrons could also transport from CB of TiO_2 to rGO sheets which inhibits the recombination of electron–hole pairs and prolongs the effective lifetimes of separated carries. The electron transport between TiO_2 and rGO can be presented by:

$$e^-_{CB} \rightarrow e^-(\text{Graphene}) \quad (8)$$

$$e^-(\text{Graphene}) + O_2 \rightarrow \cdot O_2^- \quad (9)$$

The production of $\cdot O_2^-$ would contribute to generate ·OH. The h^+_{VB} and ·OH played primary and secondary roles during the photodegradation of MB, respectively. The inhibition of recombination between electron–hole in the previous process also extended the lifetime of h^+_{VB}, enabling their reactions with H_2O to generate more ·OH which could directly oxidize MB. The reaction process can be illustrated by:

$$\cdot O_2^- + H_2O \rightarrow \cdot OH \quad (10)$$

$$h^+_{VB} + H_2O \rightarrow \cdot OH \quad (11)$$

$$\cdot OH + MB \rightarrow CO_2 + H_2O \quad (12)$$

$$h^+_{VB} + MB \rightarrow CO_2 + H_2O \quad (13)$$

Integration of Night-Time Adsorption and Day-Time Photodegradation

Under the scenario of practical application, most traditional photocatalysts are typically designed to functionalize in the daytime when sufficient light irradiations are supported.

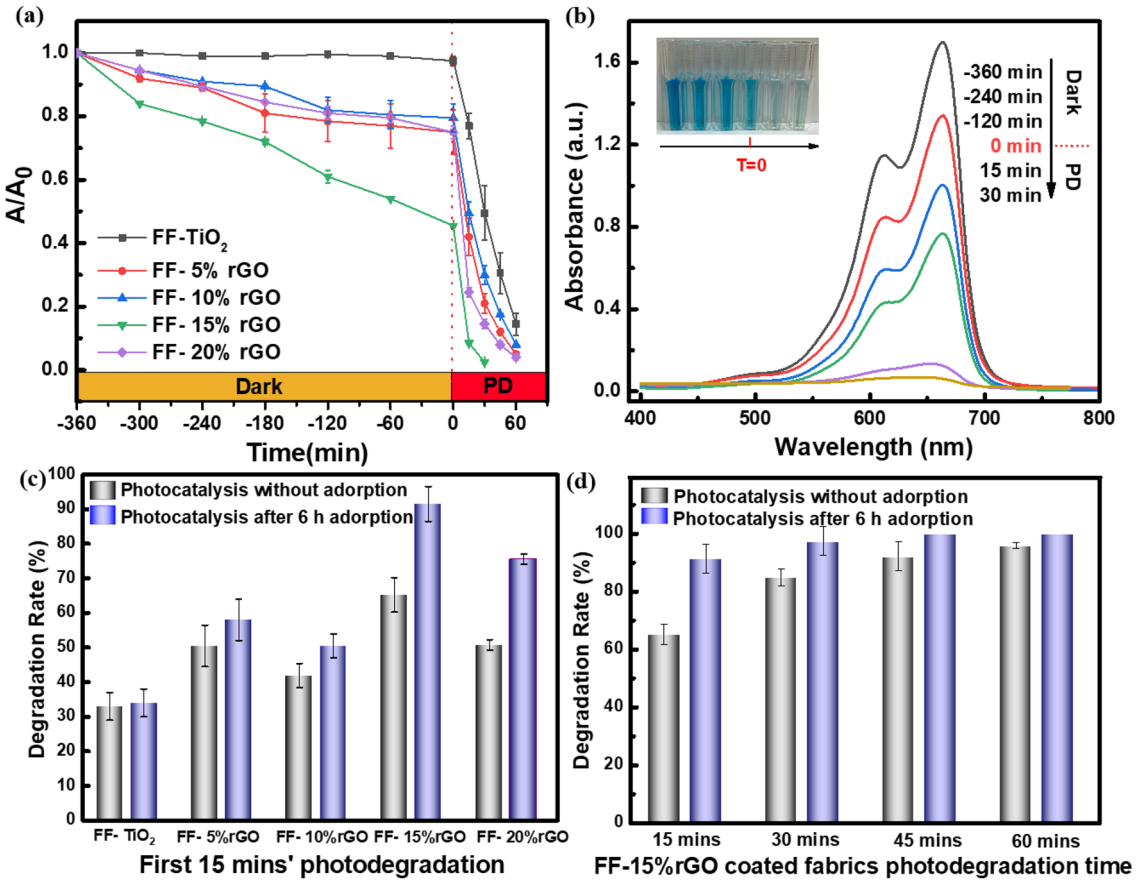

Fig. 6 **a** The integration of dark adsorption and photodegradation (PD) of MB over different fabrics. **b** The absorption spectra of MB by FF-15%rGO throughout dark adsorption and photodegradation. **c** The comparisons of degradation rates within and without 6 h' adsorption after the first 15 min' photodegradation of MB by different fabrics. **d** The comparisons of degradation rates within and without 6 h' adsorption by FF-15%rGO

The FF-rGO introduced here not only enhances the photocatalytic performance under light irradiation, it is also possessed of abundant adsorption with pollutants even without irradiation participated, especially in the nighttime when the functionalized fabrics could take full advantage of. The collaboration of day-time photodegradation and night-time adsorption optimizes the degradation efficiency of pollutants. Figure 6a shows the adsorption and degradation process of MB by FF-TiO_2 and FF-rGO during six-hour dark adsorption and one-hour photocatalysis. After six hours' adsorption, the MB concentration in solution with FF-TiO_2 did not show any declines which suggests FF-TiO_2 was not capable of absorbing MB molecules in a such short time, while the significant declines of MB concentration in solution with FF-rGO indicate the rapid absorbability of FF-rGO. The following one-hour photodegradation results show a great improvement of total degradation efficiency by FF-rGO. Figure 6b presents the UV–Vis adsorption spectra of MB aqueous during the adsorption and photocatalysis for FF-15%rGO. The sharp decline of MB concentration after 15 min' of photocatalysis demonstrates large amounts of MB molecules were aggregated and absorbed on the photocatalysts surface before photodegradation, and instantly photodegraded once the irradiation was generated.

The comparisons of photocatalytic performance within and without six-hour pre-adsorption are shown in Fig. 6c and d, respectively. At the first 15 min' photodegradation, there is a significant increase of degradation rate for FF-rGO within six-hour pre-adsorption (Fig. 6c). Typically for FF-15%rGO and FF-20%rGO, which increases 26.3% and 24.7%, respectively. The continuous photodegradation performance of FF-15%rGO shows 98% of MB has been photodegraded within 30 min if six-hour pre-adsorption was performed, while 60 min was taken to photodegrade such level of MB if no extra pre-adsorption activity was carried out (Fig. 6d). Table S4 summarizes the photodegradation efficiency of TiO_2-based materials, which indicates the remarkable degradation intensity of FF-15%rGO and

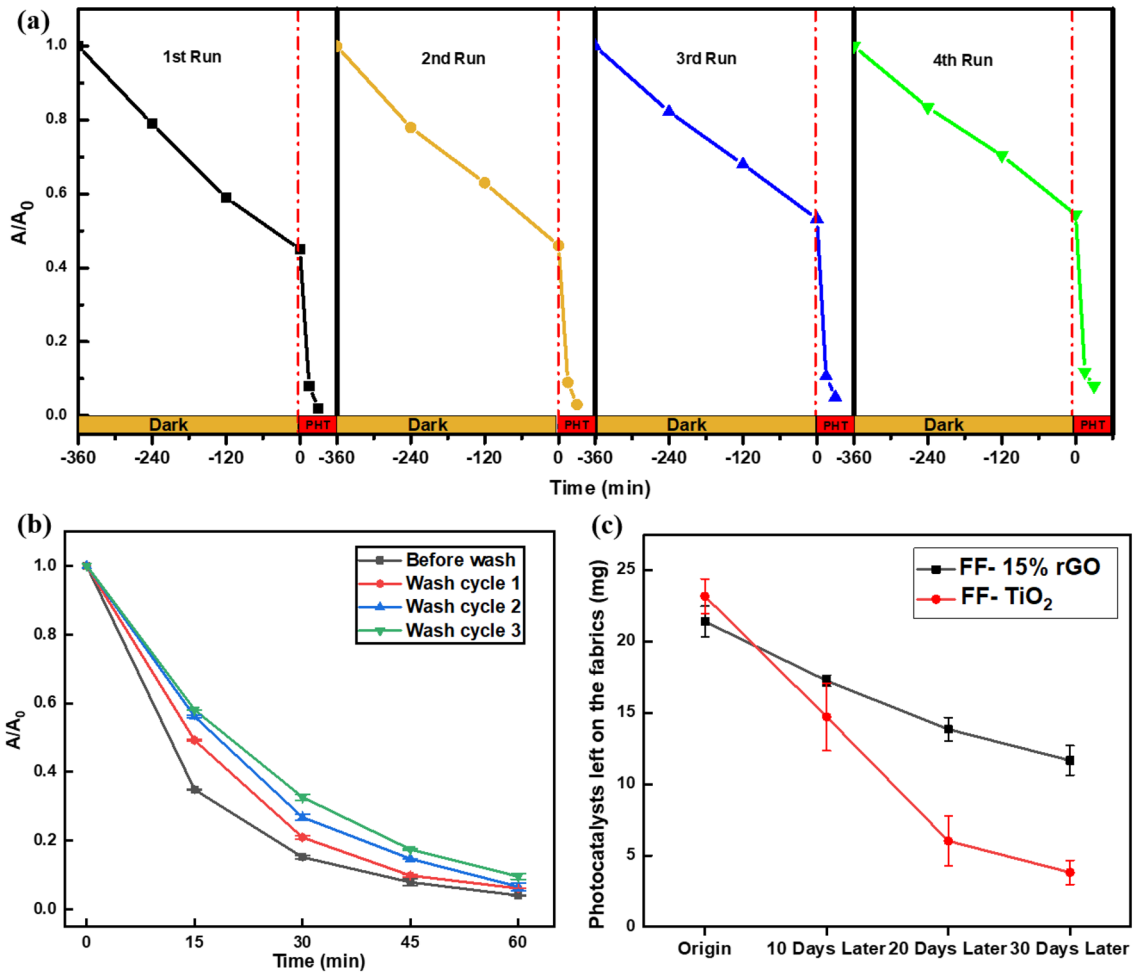

Fig. 7 Sustainability of FF-rGO. **a** Recyclability of continuous dark adsorption and photodegradation of MB by FF-15%rGO. **b** Wash test of FF-15%rGO. **c** Stability of photocatalysts on FF-15%rGO

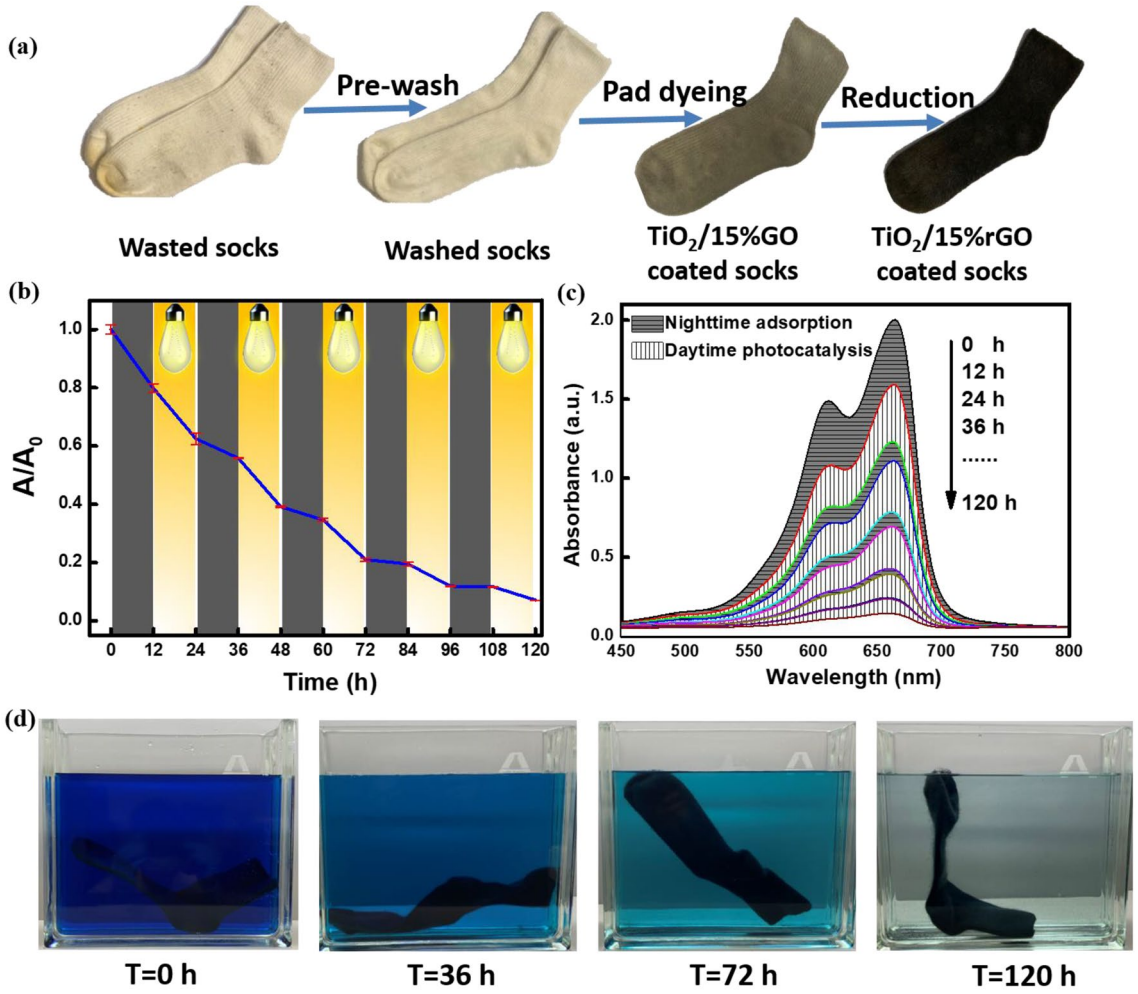

Fig. 8 Wasted socks reutilization in degradation of large-amount dyestuffs contaminations. **a** Pad dye wasted socks into TiO_2/15%rGO functionalized socks. **b** The adsorption and photodegradation of 4 L MB (10 mg/L) by functionalized sock over 120 h, 12-h nighttime adsorption and 12-h daytime photodegradation for each day. **c** The corresponding absorption spectra of MB. **d** The color change of MB solutions at 0 h, 36 h, 72 h and 120 h

significant enhancement in overall degradation intensity if extra pre-adsorption was participated. We have also analyzed the adsorbing and photocatalytic activity of FF-rGO against another organic pollutant (Rhodamine B (RhB)) in water under the same condition. The similar adsorption and photodegradation performance of FF-rGO both in MB and RhB aqueous indicate that TiO_2/rGO coated wool fabrics can be applied to water purification affected by various dyestuffs (Fig. S6).

Sustainability of FF-rGO

The stability and durability of the adsorption and photodegradation performance of FF-15%rGO were evaluated as shown in Fig. 7a. The adsorption efficiency changes from 55% for the 1st cycle to 46% for the 4th cycle, and overall degradation efficiency changes from 98% for the 1st cycle to 92% for the 4th cycle. The overall performance does not obviously deteriorate after four cycles, revealing the outstanding sustainability of FF-15%rGO.

By considering the adsorption and photocatalytic activities always take place underwater, FF-rGO requires more stability of photocatalysts on wool fabrics. We immersed FF-15%rGO into deionized water under ultrasonic treatment for 20 min for each wash cycle. The wash test indicates that the photocatalytic performance of FF-15%rGO only slightly reduced after 3 washing cycles (Fig. 7b). The 30-day soaking test proves that photocatalysts (TiO_2/rGO nanoparticles) could be more stably coated on wool fabric surface underwater compared with non-rGO incorporated photocatalysts (Fig. 7c). Such reliable stability in water is beneficial from the presence of strong bonds between rGO and TiO_2 nanoparticles, which has been confirmed in FTIR (Fig. 3e) and XPS (Fig. 3g) analysis.

Practical Application in Degradation of Large-Amount Dyestuffs Contamination

We carried out the experiment to identify the waste textile reutilization and its practical application in the degradation of large-amount dyestuffs contaminations. Figure 8a shows the wasted socks were pad dyed by TiO_2/15%rGO to achieve the optimized adsorbing and photocatalytic capacities. The functionalized sock was immersed in a tank with 4 L MB solution (10 mg/L) for 120 h (continuous alternation of 12 h' night-time adsorption and 12 h' day-time photocatalysis). More than 93% of MB in solution was removed after 120-h continuous adsorption and photodegradation (Fig. 8b). The dark grey area and light grey area in Fig. 8c represents the contribution of adsorption and photocatalysis to the overall degradation of dyestuff, respectively. The color change of MB solution in Fig. 8d and Fig. S7 suggests the effective adsorbing and degrading progress. It indicates that the integrated system of night-time adsorption and day-time photocatalysis optimizes the overall degradation of dyestuffs and have great significance to wastewater treatment.

Conclusion

In summary, we have introduced a concept to reutilize waste textiles in a green and sustainable manner through pad dyeing technology. The TiO_2/rGO functionalized fabrics exhibit decent sustainability, improved adsorbing and photocatalytic performance, displaying great potentials to solve the concerns of overproduced textiles and water contaminations arising from fast fashion industry. The FF-15%rGO presents the best adsorbing and photocatalytic performance, with a maximum adsorbing capacity of 427.35 mg/g for MB and complete photodegradation of MB (100 mL, 10 mg/L) within 60 min. Particularly, we integrated pre-adsorption and photodegradation as a combined system, which significantly shortened the photodegradation process to 30 min. Such a collaborative system takes full advantages of night-time adsorption and prominently improves the overall degradation efficiency in practical applications, paving a new route for environmental remediation.

Supplementary Information The online version contains supplementary material available at https://doi.org/10.1007/s42765-022-00192-1.

Acknowledgements This work was financially supported by the EU Horizon 2020 through project ETEXWELD-H2020-MSCA-RISE-2014 (Grant No. 644268), and the University of Manchester through the UMRI project 'Graphene-Smart Textiles E-Healthcare Network' (AA14512).

Declarations

Conflict of interest The authors declare that they have no known competing financial interests or personal relationships that could have appeared to influence the work reported in this paper.

References

1. Chen X, Memon HA, Wang Y, Marriam I, Tebyetekerwa M. Circular Economy and sustainability of the clothing and textile Industry. *Mater Circ Econ* **2021**;*3*(1):1–9.
2. Fotostock A. The price of fast fashion. *Nat Clim Chang* **2018**;*8*:1.
3. Du Z, Cheng C, Tan L, et al. Enhanced photocatalytic activity of Bi_2WO_6/TiO_2 composite coated polyester fabric under visible light irradiation. *Appl Surf Sci* **2018**;*435*:626–34.
4. Zhou D, Luo H, Zhang F, Wu J, Yang J, Wang H. Efficient photocatalytic degradation of the persistent PET fiber-based microplastics over Pt nanoparticles decorated N-doped TiO2 nanoflowers. *Adv Fiber Mater* **2022**. https://doi.org/10.1007/s42765-022-00149-4 .
5. Zhou D, Wang L, Zhang F, Wu J, Wang H, Yang J. Feasible degradation of polyethylene terephthalate fiber-based microplastics in alkaline media with Bi2O3@ N-TiO2 Z-scheme photocatalytic system. *Adv Sustain Syst* **2022**;*6*(5):2100516.
6. Li F, Wang Q, Wang X, et al. In-situ one-step synthesis of novel BiOCl/$Bi_{24}O_{31}Cl_{10}$ heterojunctions via self-combustion of ionic liquid with enhanced visible-light photocatalytic activities. *Appl Catal B-Environ* **2014**;*150*:574–84.
7. Zhang Q, Bao N, Wang X, et al. Advanced fabrication of chemically bonded graphene/TiO_2 continuous fibers with enhanced broadband photocatalytic properties and involved mechanisms exploration. *Sci Rep* **2016**;*6*(1):1–15.
8. Kowalska E, Remita H, Colbeau-Justin C, Hupka J, Belloni J. Modification of titanium dioxide with platinum ions and clusters: application in photocatalysis. *J Phys Chem C* **2008**;*112*(4):1124–31.
9. Tan LL, Chai SP, Mohamed AR. Synthesis and applications of graphene-based TiO2 photocatalysts. *Chemsuschem* **2012**;*5*(10):1868–82.
10. Schneider J, Bahnemann D, Ye J, Puma GL, Dionysiou DD, editors. Photocatalysis: fundamentals and perspectives. Royal Society of Chemistry; **2016**.
11. Wang Z, Huang B, Dai Y, et al. Crystal facets controlled synthesis of graphene@ TiO_2 nanocomposites by a one-pot hydrothermal process. *CrystEngComm* **2012**;*14*(5):1687–92.
12. Zhang X, Sun Y, Cui X, Jiang Z. A green and facile synthesis of TiO_2/graphene nanocomposites and their photocatalytic activity for hydrogen evolution. *Int J Hydrog Energy* **2012**;*37*(1):811–5.

13. Zhu Y, Meng X, Cui H, et al. Graphene frameworks promoted electron transport in quantum dot-sensitized solar cells. *ACS Appl Mater Interfaces* **2014**;*6*(16):13833–40.
14. Faraldos M, Bahamonde A. Environmental applications of titania-graphene photocatalysts. *Catal Today* **2017**;*285*:13–28.
15. Tolosana-Moranchel Á, Manassero A, Satuf ML, Alfano OM, Casas JA, Bahamonde A. Influence of TiO2-rGO optical properties on the photocatalytic activity and efficiency to photodegrade an emerging pollutant. *Appl Catal B-Environ* **2019**;*246*:1–11.
16. Sun X, Wang X, Su F, Tian M, Qu L, Perry P, Owens H, Liu X. Textile waste fibre regeneration via a green chemistry approach: a molecular strategy for sustainable fashion. *Adv Mater* **2021**;*33*(48):2105174.
17. Pandit P, Nadathur GT, Jose S. Upcycled and low-cost sustainable business for value-added textiles and fashion. In: Circular economy in textiles and apparel. Woodhead Publishing. **2019**. p. 95–122.
18. Schmidt A. Gaining benefits from discarded textiles: LCA of different treatment pathways. Nordic council of ministers. **2016**.
19. Chen J, Wu J, Sherrell P, Chen J, Wang H, Zhang W, Yang J. How to build a microplastics-free environment: strategies for microplastics degradation and plastics recycling. *Adv Sci* **2022**;*9*(6):2103764.
20. Zhai H, Xu L, Liu Z, et al. Twisted graphene fibre based breathable, wettable and washable anti-jamming strain sensor for underwater motion sensing. *Chem Eng J* **2022**;*439*:135502.
21. Zhai H, Li Y, Fan Y-Y. The effect of graphene oxides sheets on the mechanical properties of graphene fibres. *J Fiber Bioeng and Inform* **2018**;*11*(1):49–63.
22. Xu L, Liu Z, Zhai H, et al. Moisture-resilient graphene-dyed wool fabric for strain sensing. *ACS Appl Mater Interfaces* **2020**;*12*(11):13265–74.
23. Xu L, Zhai H, Chen X, et al. Coolmax/graphene-oxide functionalized textile humidity sensor with ultrafast response for human activities monitoring. *Chem Eng J* **2021**;*412*:128639.
24. Katal R, Masudy-Panah S, Tanhaei M, Farahani MHDA, Jiangyong H. A review on the synthesis of the various types of anatase TiO_2 facets and their applications for photocatalysis. *Chem Eng J* **2020**;*384*:123384.
25. Zhang L, Li Y, Zhang Q, Wang H. Hierarchical nanostructure of WO_3 nanorods on TiO_2 nanofibers and the enhanced visible light photocatalytic activity for degradation of organic pollutants. *CrystEngComm* **2013**;*15*(30):5986–93.
26. Shen J, Yan B, Shi M, Ma H, Li N, Ye M. One step hydrothermal synthesis of TiO_2-reduced graphene oxide sheets. *J Mater Chem* **2011**;*21*(10):3415–21.
27. Gómez-Navarro C, Weitz RT, Bittner AM, et al. Electronic transport properties of individual chemically reduced graphene oxide sheets. *Nano Lett* **2007**;*7*(11):3499–503.
28. Linsebigler AL, Lu G, Yates JT Jr. Photocatalysis on TiO_2 surfaces: principles, mechanisms, and selected results. *Chem Rev* **1995**;*95*(3):735–58.
29. Zhang H, Lv X, Li Y, Wang Y, Li J. P25-graphene composite as a high performance photocatalyst. *ACS Nano* **2010**;*4*(1):380–6.
30. Nguyen-Phan T-D, Pham VH, Shin EW, et al. The role of graphene oxide content on the adsorption-enhanced photocatalysis of titanium dioxide/graphene oxide composites. *Chem Eng J* **2011**;*170*(1):226–32.
31. Zhou K, Zhu Y, Yang X, Jiang X, Li C. Preparation of graphene-TiO_2 composites with enhanced photocatalytic activity. *New J Chem* **2011**;*35*(2):353–9.
32. Wang C, Shao C, Zhang X, Liu Y. SnO2 nanostructures-TiO_2 nanofibers heterostructures: controlled fabrication and high photocatalytic properties. *Inorg Chem* **2009**;*48*(15):7261–8.
33. Huang Q, Tian S, Zeng D, et al. Enhanced photocatalytic activity of chemically bonded TiO2/graphene composites based on the effective interfacial charge transfer through the C-Ti bond. *ACS Catal* **2013**;*3*(7):1477–85.
34. He YQ, Zhang NN, Wang XD. Adsorption of graphene oxide/chitosan porous materials for metal ions. *Chin Chem Lett* **2011**;*22*(7):859–62.
35. Langmuir I. The adsorption of gases on plane surfaces of glass, mica and platinum. *J Am Chem Soc* **1918**;*40*(9):1361–403.
36. Freundlich H. Über die adsorption in lösungen. *Z Phys Chem* **1907**;*57*(1):385–470.
37. An W, Cui W, Liang Y, Hu J, Liu L. Surface decoration of BiPO4 with BiOBr nanoflakes to build heterostructure photocatalysts with enhanced photocatalytic activity. *Appl Surf Sci* **2015**;*351*:1131–9.
38. Corbett JF. Pseudo first-order kinetics. *J Chem Educ* **1972**;*49*(10):663.
39. Zhang L, Mohamed HH, Dillert R, Bahnemann D. Kinetics and mechanisms of charge transfer processes in photocatalytic systems: a review. *J Photochem Photobiol C: Photochem Rev* **2012**;*13*(4):263–76.

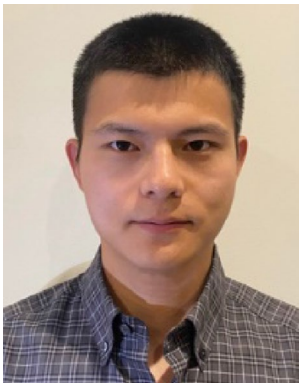

Heng Zhai received his B.Sc degree in Textile Science and Technology from The University of Manchester in 2017. After that, he was continuous to a straight doctoral study in the same organization. His Ph.D. research mainly focuses on the fabrication of functional graphene and graphene fiber-based composites for wearable electronics and environmental remediation.

Zekun Liu recieved his Ph.D. degree at Department of Materials, The University of Manchester, United Kingdom. He is now working as a Research Associate at Nuffield Department of Orthopaedics, Rheumatology and Musculoskeletal Sciences, University of Oxford. His research interests include nanomaterials and functionalized materials for the development of advanced composites, functional clothes, biomedical devices, and flexible electronics such as sensors, batteries, solar cells, and generators.

Lulu Xu currently works as a research fellow at Wellcome-EPSRC Centre for Interventional and Surgical Sciences (WEISS), University College London (UCL). She received her Ph.D. degree from Manchester University in 2020. Her main research was mainly focused on the development of soft and flexible electronics for wearable applications.

Ting Liu received his B.Sc degree in Material and science from the Hefei University of Technology in 2015. After that, he finished his MSc study about advanced engineering materials from the University of Manchester. Then, he was continuous to PhD research at the same university mainly focuses on the fabrication of porous PLLA/TiO_2 fibrous membranes and their applications in the environmental remediations and antibacterial.

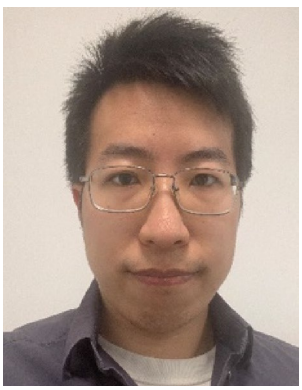

Yangyang Fan received his BSc degree in Polymer Materials Science and Engineering from Donghua University in 2014. He received master's degree in the University of Manchester in 2015. He started his PhD study in 2016 in the University of Manchester. His PhD research mainly focused on the fabrication of graphene fibres, mechanical and electrical behaviour of graphene fibres, and wearable electronics.

Lu Jin received a BEng degree in textile engineering from Tianjin Polytechnic University, Tianjin, China, MS degree in Polymer Science and Engineering from Dankook University, South Korea, and Ph.D. in Textile Science and Technology from The University of Manchester, Manchester, United Kingdom, in 2006, 2009 and 2021, respectively. His research interests include dry electrodes, unimodal strain sensors, airflow transducers and protective clothing.

Ruihan Dong accomplished her B.E. in Textile engineering from Soochow University in 2020. After that, she received her M.S. from the school of materials, the University of Manchester. Her research interests include wearable multifunctional sensors, flexible carbon materials, human-machine interface applications, and advanced textile materials.

Yangpeiqi Yi is currently a Ph.D. student in Department of Materials, The University of Manchester, United Kingdom. His current research mainly focuses on ink-based processes for breathable and flexible electronics.

Yi Li is a full professor and chair in Textile Science and Engineering in the University of Manchester. He is a Life-Fellow of Royal Society of Art and International Biographical Association and Fellow of the Textile Institute. He is the Chairman of Textile Bioengineering and Informatics Society, deputy council chairman of International Digital Health and Intelligent Materials Innovation Alliance, and board chair of Fashion Big Data Foundation. His research focuses advancement of emerging cross-disciplinary science and engineering of how to design and engineer biomaterials, drug delivery systems, medical devices, smart e-textiles, intelligent wearables for human psychological and physiological needs.